A Human subunits

		TMD4
α	EWKYVAMVMDH	ILLGVFML
β	DWQFVAMVVDR	LFLWTFII
δ	EWFLVGRVLDR	VCFLAMLS
γ	SWNRVARTVDR	LCLFVVTP
ε	DWVRMGNALDN	ICFWAALV

ε subunits

		TMD4
Xenopus	NWILIGKVLDV	LCFWVALP
Mouse	DWVRMGKALDN	VCFWAALV
Rat	DWVRMGKALDN	VCFWAALV
Bovine	DWVRMGKALDS	ICFWAALV
Human	DWVRMGNALDN	ICFWAALV

B Mutations in ε subunit

	TMD4	Length Change	Charge Change
human ε	DWVRMGNALDN ICFWAALV	0	0
εN436del	DWVRMGNALD- ICFWAALV	-1	-
εD435del	DWVRMGNAL-N ICFWAALV	-1	0
εN436R	DWVRMGNALDR ICFWAALV	0	+
εN436D	DWVRMGNALDD ICFWAALV	0	-
εDN435del	DWVRMGNAL-- ICFWAALV	-2	0

C Mutations in non-ε subunits

	TMD4
human α	EWKYVAMVMDH ILLGVFML
αH408del	EWKYVAMVMD- ILLGVFML
human β	DWQFVAMVVDR LFLWTFII
βR446del	DWQFVAMVVD- LFLWTFII
human δ	EWFLVGRVLDR VCFLAMLS
δR450del	EWFLVGRVLD- VCFLAMLS

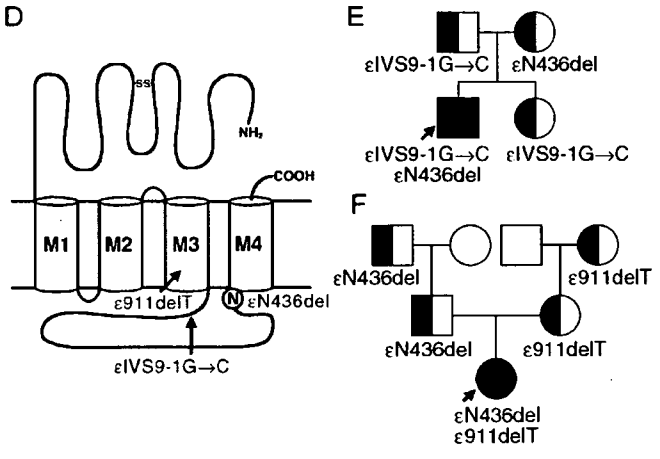

Fig. 3 (**A**) Multiple alignment of the carboxy-terminal segment of the M3–M4 loop and part of the M4 domain of AChR subunits. (**B**) Naturally occurring (εN436del) and artificial mutations in ε subunit expressed in HEK cells. Rightmost columns indicate the number of deleted codons and the charge of the C-terminal residue of the M3–M4 loop. (**C**) Artificial mutations in the α, β and δ subunits expressed in HEK cells. (**D**) Scheme of the ε subunit showing positions of mutations in patients 1 and 2. (**E**) Family analysis in patient 1. (**F**) Family analysis in patient 2.

The second mutation in patient 1 is a previously reported splice site mutation at the 3′ end of intron 9 (εIVS9-1G→C) that alters the canonical AG to AC at the splice acceptor site (Fig. 3D). The mutation causes retention of intron 9, predicting 67 missense amino acids followed by a stop codon. The genetically engineered aberrantly spliced transcript is not expressed on the surface of HEK cells (Ohno *et al.*, 2003). The second mutation in patient 2 is a previously reported frameshifting null mutation in the M3 domain of the ε subunit (ε911delT) (Brengman *et al.*, 2000; Sieb *et al.*, 2000) (Fig. 3D).

Family analysis in both patients indicates that the observed mutations are heteroallelic and recessive (Fig. 3E and F). Because εIVS9-1G→C and ε911delT are null mutations, εN436del determines the phenotype of both patients.

Expression studies of εN436del-AChR expressed in HEK cells

To determine whether εN436del hinders the amount of AChR expressed on the cell surface, we engineered εN436del into the human ε subunit and coexpressed it with complementary wild-type α, β and δ subunits in HEK cells. As a control, we coexpressed α, β and δ subunits in the absence of the ε subunit. Measurement of [^{125}I]α-bgt binding revealed εN436del-AChR reduced surface expression to ~50% of wild-type, while that of ε-omitted $\alpha_2\beta\delta_2$-AChR was ~38% of wild-type (Fig. 4A).

To distinguish between lack of incorporation and reduced expression of the mutant ε subunit, we measured ACh binding at steady state by competition against the initial rate of [^{125}I]α-bgt binding (Sine and Taylor, 1979). Wild-type $\alpha_2\beta\delta\varepsilon$ pentamers bind ACh in a monophasic manner, whereas ε-omitted $\alpha_2\beta\delta_2$ pentamers bind ACh in a biphasic manner (Fig. 4B) (Ohno *et al.*, 1996). εN436del-AChR binds ACh in a monophasic manner like wild-type AChR (Fig. 4B), indicating that the mutant subunit incorporates into most if not all cell surface pentamers. The apparent dissociation constant of εN436del-AChR for ACh was very similar to that of wild-type AChR (Fig. 4B).

To examine kinetic effects of εN436del, we recorded single-channel currents from human embryonic kidney (HEK) cells expressing εN436del-AChR or wild-type AChR activated by a low concentration of ACh (50 nM). Open interval and burst duration histograms of both wild-type and mutant AChRs showed three components, presumably corresponding to two brief mono-liganded open states and one long diliganded open state. Mean durations of diliganded openings are reduced to 46% of wild type by εN436del, and those of the corresponding bursts are reduced to 38% (Table 2 and Fig. 5A and B).

The effects of εN436del are caused by shortening of the M3–M4 loop

The εN436del mutation shortens the M3–M4 loop and at the same time shifts a negatively charged aspartic acid residue to

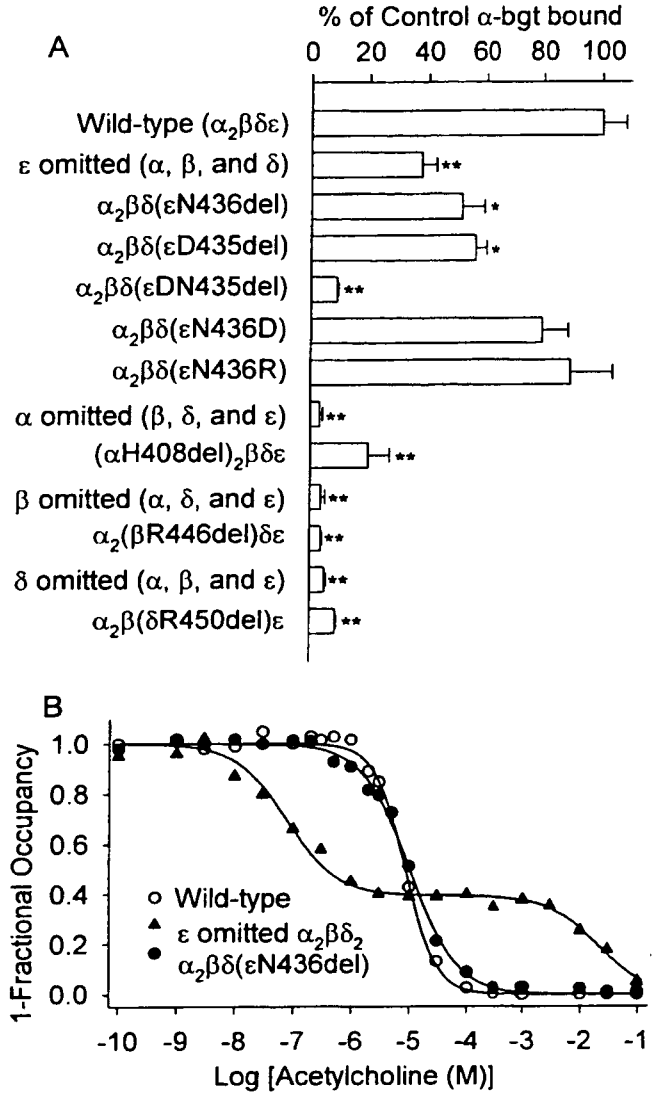

Fig. 4 (**A**) [^{125}I]α-bgt binding to surface receptors on intact HEK cells transfected with the indicated AChR subunits. The results are normalized for α-bgt binding to wild-type AChR and represent the mean and SD of three to six experiments. $^*P < 0.05$; $^{**}P < 0.01$, compared with wild-type AChR. (**B**) ACh binding to intact HEK cells transfected with indicated AChR subunits determined by competition against the initial rate of [^{125}I]α-bgt binding. Curves are fitted to the Hill equation (see Methods). $K_{ov} = 8.69 \times 10^{-6}$, $n = 1.65$ for wild-type AChR; $K_{ov} = 1.03 \times 10^{-5}$, $n = 1.07$ for εN436del-AChR; and $K_A = 7.73 \times 10^{-8}$, $K_B = 2.22 \times 10^{-2}$, $fract_A = 0.61$ for ε-omitted AChR.

the N-terminal end of M4. To determine whether either or both effects reduce expression or alter activation of AChR, we engineered four site-directed mutants (Fig. 3B) and expressed each together with complementary wild-type subunits in HEK cells.

The first engineered mutant, εD435del, shortens the M3–M4 loop by a single residue, without shifting a negative charge against M4 (Fig. 3B). This mutation reduces surface expression of AChR to ~56% of wild-type (Fig. 4A) and decreases the mean durations of the major components of channel openings and bursts (Table 2 and Fig. 5C) to ~65 and ~50% of wild-type, respectively. The second engineered mutant, εDN435del, which removes two residues from the M3–M4 loop (Fig. 3B), reduces AChR expression to ~10% of wild-type, and decreases the mean durations of the longest components of channel openings and bursts to ~65 and ~55% of wild-type, respectively (Table 2 and Fig. 5F). The third and fourth engineered mutants, εN436R and εN436D, do not shorten the M3–M4 loop but position a positive or negative charge next to M4 (Fig. 3B). Neither mutant has an appreciable effect on AChR surface expression (Fig. 4A) or channel kinetics (Table 2 and Fig. 5D and E). Thus, the effects of εN436del on AChR expression and channel kinetics can be attributed to shortening of the M3–M4 loop and not to shift of a negative charge adjacent to M4.

Deletion of equivalent residues in non-ε subunits

To determine whether the effects of deleting a C-terminal residue of the M3–M4 loop are subunit specific, we constructed corresponding deletion mutants of the α (αH408del), β (βR446del) and δ (δR450del) subunits (Fig. 3C). The β and δ deletion mutants reduce surface expression of AChR to ~5% of wild-type (Fig. 4A) and shorten channel opening events by about the same amount as εN436del (Table 2 and Fig. 5H and I). The αH408del mutation reduces expression of AChR to ~20% of wild-type (Fig. 4A) and, in striking contrast to the β and δ deletion mutants, prolongs the dominant component of open intervals ~3.5-fold and that of bursts ~13.5-fold (Table 2 and Fig. 5G).

Because HEK cells bound similar low levels of [^{125}I]α-bgt after transfection with δR450del-AChR, $\alpha_2\beta\varepsilon_2$-AChR, βR446del-AChR and $\alpha_2\beta\varepsilon_2$-AChR (Fig. 4A), the channel events recorded from the transfected HEK cells could have arisen from δ-omitted or β-omitted receptors rather than from δR450del-AChR or βR446del-AChR. To test this possibility, we expressed either δ- or β-omitted AChRs in HEK cells in each of three different experiments and searched for channel openings in 30 and 31 patches, respectively, but detected no channel openings. Therefore, it is unlikely that either δ- or β-omitted AChRs, if present, are functional.

Activation kinetics of εN436del-AChR and αH408del-AChR

To determine the mechanism by which the εN436del receptor shortens and the α408Hdel receptor prolongs channel opening events, we examined their kinetics of activation at desensitizing concentrations of ACh (see Methods). Wild-type and εN436del-AChRs generated well-defined clusters of openings at ACh concentrations as low as 10 and 20 μM, respectively, but αH408del-AChR produced clusters of openings even at 0.3 μM ACh, indicating an enhanced propensity of receptors containing the mutant α subunit to become desensitized (Fig. 6, left column).

Table 2 *Single-channel recordings of wild-type and mutant AChRs expressed in HEK cells*

	Open interval			Bursts		
	τ_1 (ms) (a_1)	τ_2 (ms) (a_2)	τ_3 (ms) (a_3)	τ_1 (ms) (a_1)	τ_2 (ms) (a_2)	t_3 (ms) (a_3)
Wild-type	0.037 ± 0.033[a]	0.31 ± 0.050	1.35 ± 0.05	0.036 ± 0.002[b]	0.47 ± 0.06	3.31 ± 0.12
	(0.17 ± 0.02)	(0.27 ± 0.04)	(0.67 ± 0.04)	(0.24 ± 0.021)	(0.21 ± 0.03)	(0.58 ± 0.04)
εN436del	0.031 ± 0.0033[c]	0.24 ± 0.06[d]	0.62 ± 0.03	0.036 ± 0.005[c]	0.30 ± 0.03[e]	1.24 ± 0.092
	(0.15 ± 0.01)	(0.46 ± 0.03)	(0.76 ± 0.09)	(0.23 ± 0.022)	(0.43 ± 0.06)	(0.78 ± 0.07)
εD435del	ND	0.20 ± 0.09	0.87 ± 0.05	ND	0.25 ± 0.08	1.66 ± 0.15
		(0.24 ± 0.08)	(0.76 ± 0.08)		(0.35 ± 0.09)	(0.65 ± 0.09)
εDN435del	ND	0.20 ± 0.02	0.88 ± 0.04	ND	0.31 ± 0.07	1.82 ± 0.10
		(0.34 ± 0.06)	(0.66 ± 0.06)		(0.48 ± 0.06	(0.52 ± 0.06)
εN436R	0.058 ± 0.014	0.39 ± 0.08[b]	1.31 ± 0.12	0.052 ± 0.01	0.45 ± 0.13[f]	3.33 ± 0.44
	(0.16 ± 0.008)	(0.29 ± 0.55)	(0.70 ± 0.07)	(0.32 ± 0.02)	(0.25 ± 0.01)	(0.53 ± 0.07)
εN436D	0.054 ± 0.014[b]	0.39 ± 0.10	1.15 ± 0.13	0.034 ± 0.006[f]	0.55 ± 0.15	3.03 ± 0.15
	(0.14 ± 0.07)	(0.23 ± 0.48)	(0.72 ± 0.08)	(0.20 ± 0.08)	(0.26 ± 0.07)	(0.62 ± 0.10)
βR446del	0.032 ± 0.0024[f]	ND	0.73 ± 0.12	0.027 ± 0.004[f]	ND	1.40 ± 0.29
	(0.12 ± 0.0009)		(0.93 ± 0.03)	(0.11 ± 0.03)		(0.84 ± 0.07)
δR450del	0.041[c]	0.33 ± 0.06[f]	0.73 ± 0.12	0.050[c]	0.49 ± 0.12[b]	1.13 ± 0.18
	(0.30)	(0.49 ± 0.11)	(0.60 ± 0.12)	(0.24)	(0.46 ± 0.10)	(0.70 ± 0.10)
αH408del	0.031 ± 0.0030	0.98 ± 0.21	4.70 ± 0.76	0.067 ± 0.02	1.33 ± 0.29	44.76 ± 3.56
	(0.20 ± 0.03)	(0.16 ± 0.03)	(0.68 ± 0.05)	(0.41 ± 0.05)	(0.21 ± 0.05)	(0.38 ± 0.05)

Values indicate mean ± SE. τ_n and a_n indicate time constants and fractional histogram areas. Wild-type, εN436del, εD435del, εN436R, εN436D and αH408del were recorded with 50 nM ACh from 21, 11, 3, 5, 5 and 6 patches, respectively; εDN435del, βR446del and δR450del were recorded with 1 μM ACh from 3, 5 and 7 patches respectively. Membrane potential = −80 mV. [a, b, c, d, e, f]Either the first or the second component was not detected at 12, 3, 6, 7, 8 and 2 patches, respectively.

For both wild-type and εN436del-AChRs, the longest closed-time component shifted to shorter durations with increasing ACh concentration (Fig. 6, central column). The open times of the εN436del receptors were briefer and those of the αH408del receptor longer compared with wild-type (Fig. 6, right column). Dwell times for wild-type and mutant receptors show typical dependence on ACh concentration: closings become briefer with increasing ACh concentration, and the major component of openings changes little across ACh concentrations.

To determine the consequences of the mutations on rate constants underlying receptor activation, we analysed the global set of open and closed dwell times according to scheme 1:

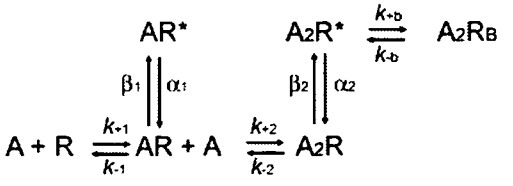

In this scheme, two agonists (A) bind to the receptor (R) with association rate constants k_{+1} and k_{+2}, and dissociate with rate constants k_{-1} and k_{-2}. Receptors occupied by one agonist open with rate β_1 and close with rate α_1, while receptors occupied by two agonists open with rate β_2 and close with rate α_2. Asterisks indicate open states and R_B indicates the blocked state of the receptor. At high ACh concentrations, ACh blocks the open channel with rate k_{+b}, and the channel unblocks with rate k_{-b}. The fitted rate constants allow calculation of the equilibrium dissociation constants ($K_n=k_{-n}/k_{+n}$, $K_B=k_{-b}/k_{+b}$) and the channel gating equilibrium constants ($\theta_n=\beta_n/\alpha_n$). This scheme allows for only two open states, whereas low-concentration recordings (Fig. 5 and Table 2) had revealed three open states. However, at the high concentrations of ACh required to elicit clusters of channel events due to a single channel, only two components of openings are observed, presumably because the briefest class of monoliganded openings occurs too infrequently to be identified.

Scheme 1 provided a good description of the closed and open intervals for wild-type and εN436del receptors but did not provide a satisfactory description of the closed intervals for the αH408del mutant. The chief problem was complexity of the closed duration distribution, which exhibited at least one more component than accounted for by scheme 1. We therefore examined alternative scheme 2, which incorporated an additional closed state branching from the diliganded open state:

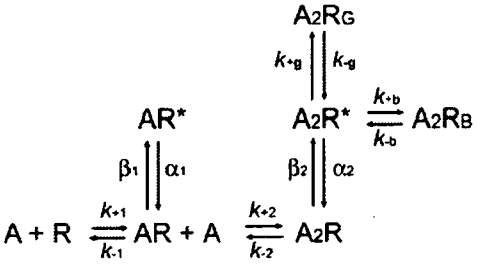

An analogous brief closed state was suggested by Elenes and Auerbach (2002) for wild-type mouse muscle AChR, and by Hatton and colleagues in describing the activation of the εL221F slow-channel mutation (Hatton *et al.*, 2003), both groups suggesting that it corresponded to a short-lived

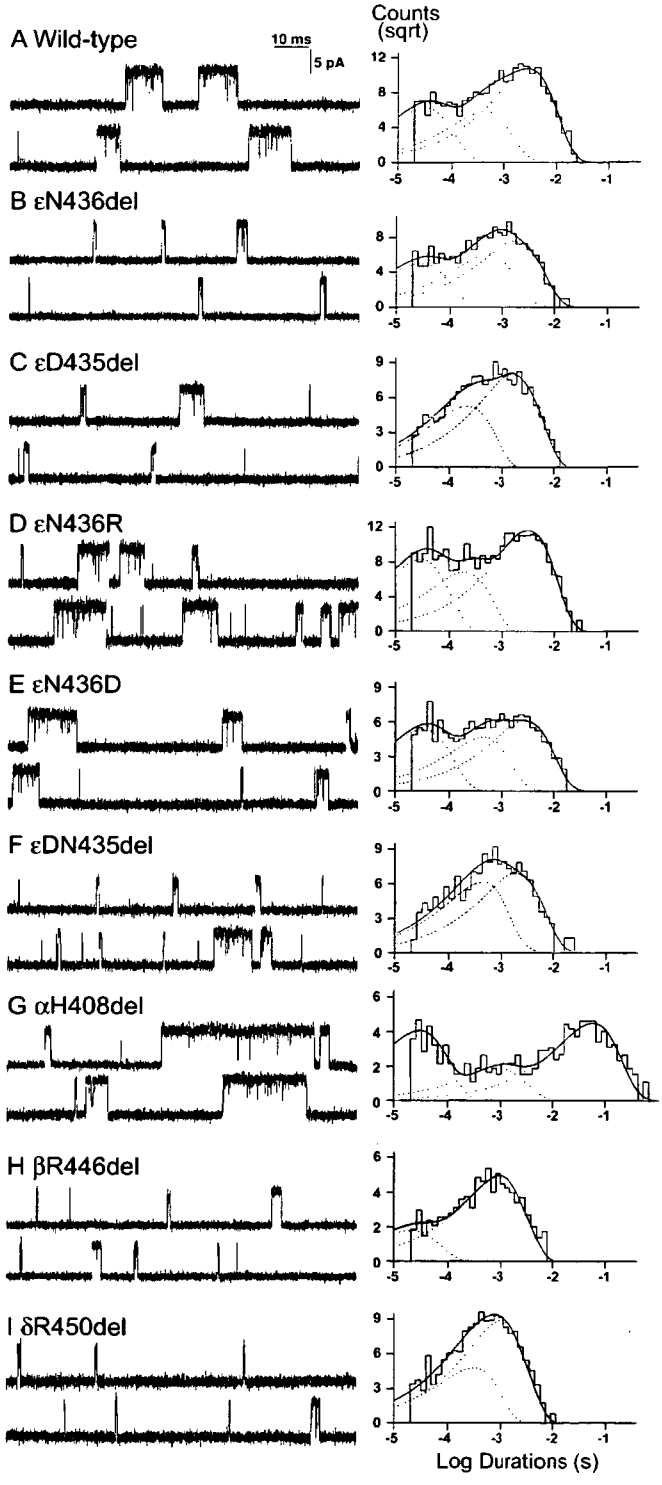

Fig. 5 (*Left*) AChR channel events elicited by 50 nM (A, B, C, D, E, G) or 1 μM (F, H, I) ACh from HEK cells transfected with indicated AChR subunits. (*Right*) Burst duration histograms fitted to the sum of exponentials.

desensitized state. Schemes 1 and 2 provided equally satisfactory fits and similar rate constants for the human wild-type and εN436del receptors. To compare activation kinetics of wild type and mutant receptors, we analysed our data according to scheme 2 (Table 3).

Table 3 *Kinetic parameters of wild-type and mutant AChRs expressed in HEK cells*

Rate constant	Wild-type	εN436del	αH408del
k_{+1}	59 ± 6	32 ± 2	72 ± 5
k_{-1}	953 ± 57	414 ± 44	336 ± 41
k_{+2}	77 ± 2	54 ± 1	369 ± 35
k_{-2}	10 300 ± 170	15 800 ± 327	2880 ± 153
β_1	146 ± 13	556 ± 29	194 ± 21
α_1	3240 ± 323	5520 ± 243	19 200 ± 1321
β_2	52 800 ± 1190	42 300 ± 1960	81 900 ± 3037
α_2	2100 ± 69	4000 ± 139	704 ± 39
k_{+g}	20 ± 1	51 ± 6	52 ± 3
k_{-g}	802 ± 62	959 ± 86	10 500 ± 778
k_{+b}	17 ± 2	25 ± 3	ND
k_{-b}	84 100 ± 1719	73 400 ± 5360	ND
K_1 (μM)	16	13	5
K_2 (μM)	133	293	8
θ_1	0.045	0.100	0.010
θ_2	25	11	116
K_B (mM)	4.95	2.93	–
K_G	40	19	202
Predicted burst length (ms)	3.12	1.26	42.40
Low-concentration burst length (ms)	3.31	1.24	44.76

Association rates and k_{+b} are in $\mu M^{-1} s^{-1}$; all other rate constants are in s^{-1}. Gating equilibrium constants θ_n are the ratios β_n/α_n. The predicted burst length was derived from a rate constant Q matrix (Colquhoun and Sigworth, 1995; Colquhoun and Hawkes, 1995). $K_G = k_{-g}/k_{+g}$. ND = not detected.

The fitted rate constants in Table 3 indicate the following functional consequences of the εN346del mutant: by decreasing k_{+2} and increasing k_{-2}, it increases K_2 ~2.2-fold, thus decreasing the affinity of the diliganded closed receptor for ACh; and by decreasing β_2 and increasing α_2, it decreases the gating efficiency of the diliganded receptor (θ_2) ~2.3-fold. The fitted rate constants were used to predict burst duration at very low concentrations of agonist, which agreed very well with the independently determined burst duration obtained at 50 nM ACh (Table 3). Overall, the εN346del burst duration is reduced to 40% of wild-type, and the mutant receptor has mild fast-channel properties (Engel *et al.*, 2003).

The αH408del mutation, on the other hand, has opposite effects to εN346del: by increasing k_{+1} and k_{+2} and decreasing k_{-1} and k_{-2}, it decreases K_1 3-fold and K_2 ~17-fold, thus markedly enhancing both monoliganded and diliganded closed state affinities; by increasing β_2 ~1.5-fold and slowing α_2 ~3.0-fold, it increases the gating efficiency of the diliganded receptor ~5-fold. Again, burst duration predicted by the fitted rate constants agreed well with the independently determined burst duration obtained at 50 nM ACh (Table 3). Burst duration increases ~14-fold, and the αH408del receptor has pronounced slow-channel properties (Engel, *et al.*, 2003).

Figure 7 shows plots of open probabilities (P_{open}) within defined clusters of channel events at different concentrations

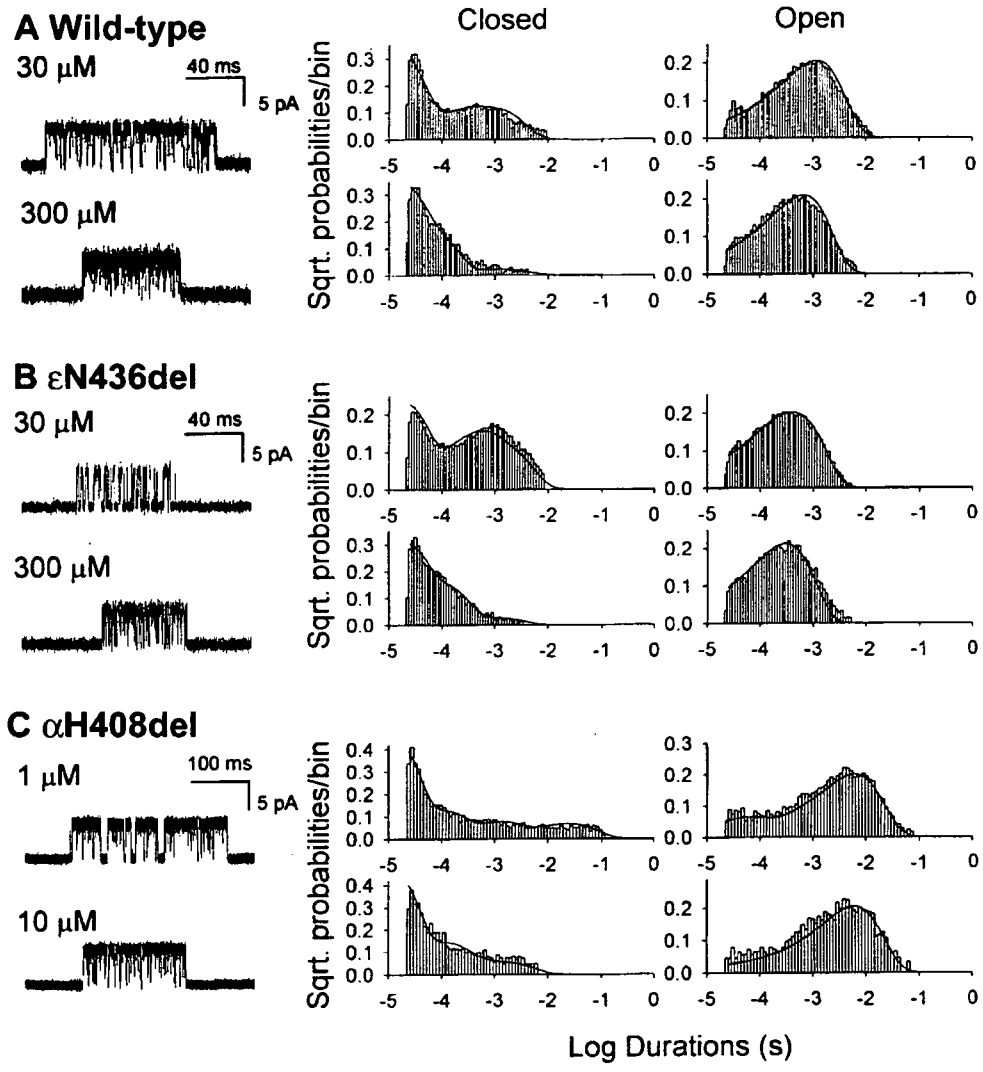

Fig. 6 Kinetics of activation of wild-type (**A**), εN436del- (**B**), and αH408del- (**C**) AChR. (*Left column*) individual clusters of single-channel currents recorded at indicated ACh concentrations from HEK cells. (*Centre and right columns*) Corresponding histograms of closed and open durations with superimposed probability density functions for scheme 2 of receptor activation for the entire range of ACh concentrations. Table 3 shows the fitted rate constants.

of ACh for the wild-type, εN436del-AChR and αH408del receptors. The plotted points are well described by the theoretical P_{open} curve computed from the rate constants determined by fitting scheme 2 to the dwell times (Fig. 7). The P_{open} curve for εN436del receptor is right-shifted with respect to wild-type, indicating a 3.5-fold decreased probability of opening at the EC_{50}. In contrast, the P_{open} curve for the αH408del receptor is left-shifted with respect to wild-type, indicating a ~31-fold increased probability of opening at EC_{50}.

Discussion

Phenotypic consequences of εN436del

Both CMS patients carry the εN436del mutation plus a null mutation in the second ε allele; therefore, εN346del determines the phenotype. EP studies demonstrate severe AChR deficiency, compensatory expression of fetal-type γ-AChR, and short opening events of the expressed adult ε-AChRs. Expression of γ-AChR at the EP has been documented with low-expressor or null mutations of the ε subunit, where it probably serves as a means of phenotypic rescue (Engel *et al.*, 2003). Because the number of AChRs at both patients' EPs is only ~10% of normal and most expressed AChRs harbour the fetal γ subunit, neuromuscular transmission is primarily compromised by the AChR deficiency, and this is compounded by the fast-channel kinetics of the εN436del-AChRs.

Expression of εN436del-AChR in HEK cells was 50% of wild-type. Higher AChR expression in HEK cells than at the EP has been observed previously with other low-expressor missense mutations of AChR (Milone *et al.*, 1998; Ohno *et al.*, 1997; Shen *et al.*, 2002; Wang *et al.*, 1999). This may be due to differences in the rate of synthesis or destruction of the mutant receptor in muscle fibres versus HEK cells. Interaction with the cytoplasmic anchoring protein rapsyn, absent in HEK cells, may also be compromised by the mutant receptors at the EP.

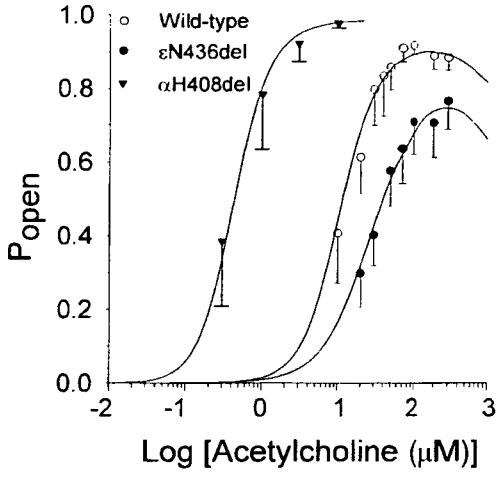

Fig. 7 Open probability (P_{open}) as a function of ACh concentration. Symbols represent mean P_{open} computed for 18–311 clusters per patch. Error bars indicate the standard deviation. Smooth curves are the predicted P_{open} computed from the rate constants in Table 3. Note the right shift of the curve for εN436del and δR450del, and the left shift of the curve for αH408del.

Expression of AChRs harbouring C-terminal deletion mutants of M3–M4 loops

All three C-terminal deletion mutants of the ε M3–M4 loop (εN436del, εD435del and εDN435del) as well as the corresponding deletion mutants of the α (α408Hdel), β (βR446del) and δ (δR450del) subunits curtail surface expression of AChR, whereas the two C-terminal charge mutants of the ε M3–M4 loop (εN436D or εN436R) do not; therefore the decreased AChR expression probably stems from shortening of the M3–M4 loop. Decreased AChR expression, in turn, may stem from abnormal folding and accelerated destruction of nascent peptides in the endoplasmic reticulum, or because C-terminal residues of the M3–M4 loops are required for efficient subunit assembly, or both.

Activation kinetics of C-terminal deletion mutants of the M3–M4 loops

Scheme 1 described well the kinetics of activation the wild-type and εN436del receptors, but did not account for all closed states of the αH408del receptor. We therefore explored an alternative scheme (scheme 2) that allowed an additional closed state connected to the open state of the receptor (A_2R_G); scheme 2 described both closed and open times of the αH408del receptor. Interestingly, applying scheme 2 to the wild-type and the εN436del receptors did not significantly alter the rate constants of activation or improve the likelihood of the fitted parameters compared to scheme 1. This finding differs from that in the mouse receptor, where allowing a non-conducting gap to arise from the diliganded open state improved the quality of the fit (Elenes and Auerbach, 2002). The functional significance of the A_2R_G state is not known; it may represent a brief desensitized state of the receptor (Salamone *et al.*, 1999), but that the dwell in the A_2R_G state is ~13 times shorter for the desensitization prone αH408del receptor than for the wild-type or the εN436del receptor appears inconsistent with this interpretation.

The results shed new light on the structure–function relationships of the AChR. In particular, the M3–M4 linker has been shown to be a primary determinant of the fetal-to-adult kinetic switch, conferred by change from γ to ε subunits (Bouzat *et al.*, 1994), as well as a determinant of the fidelity of channel gating (Milone *et al.*, 1998; Wang, *et al.*, 2000). The collective studies point to γ and ε as subunits that specifically contribute to activation kinetics, but the present work is the first to show a contribution of the M3–M4 loop of the α subunit. The single residue deletion from the α subunit prolongs channel activation episodes and enhances desensitization to extents comparable to severe slow channel mutations. The enhanced activation is attributed to enhanced affinity of ACh for the resting closed state of the receptor as well as to enhanced gating. Both the ACh binding site (Celie *et al.*, 2004) and the channel gate (Miyazawa *et al.*, 2003) are distant from the M3–M4 linker, indicating an allosteric contribution of the M3–M4 loop of the α subunit to receptor function. Thus, combined clinical, morphological, electrophysiological and genetic studies of our two patients unravelled the pathophysiological basis of a CMS. Further experimentation revealed subunit-specific contributions of C-terminal residues of the M3–M4 loops of AChR that allosterically affect gating of the ion channel and ACh occupancy of the more distant binding site.

Acknowledgements

This work was supported by NIH grants to A. G. E. (NS-6277) and to S. M. S. (NS-31744) and by a Muscular Dystrophy Association Grant to A. G. E.

References

Bouzat C, Bren N, Sine SM. Structural basis of different gating kinetics of fetal and adult acetylcholine receptors. Neuron 1994; 13: 1395–402.

Brengman JM, Ohno K, Milone M, Friedman RL, Feldman RG, Engel AG. Identification and functional characterization of eight novel acetylcholine receptor mutations in six congenital myasthenic syndrome kinships. Neurology 2000; 54 (Suppl. 3): A182–3.

Celie PH, van Rossum-Fikkert SE, van Dijk WJ, Brejc K, Smit AB, Sixma TK. Nicotine and carbamycholine binding to nicotinic acetylcholine receptors as studied in AChBP crystal structures. Neuron 2004; 41: 907–14.

Colquhoun D, Hawkes AG. A Q-matrix cookbook: how to write only one program to calculate the single-channel and macroscopic predictions for any kinetic mechanism. In: Sakmann B, Neher E, editors. Single-channel recording. New York: Plenum Press; 1995. p. 589–633.

Colquhoun D, Sakmann B. Fast events in single channel currents activated by acetylcholine and its analogues at the frog muscle end-plate. J Physiol (Lond) 1985; 369: 501–57.

Colquhoun D, Sigworth FJ. Fitting and statistical analysis of single-channel records. In: Sakmann B, Neher E, editors. Single-channel recording. New York: Plenum Press; 1995. p. 483–587.

Croxen R, Young C, Slater C, Haslam S, Brydson M, Vincent A, et al. Endplate γ- and ε subunit mRNA levels in AChR deficiency syndrome due to ε subunit null mutations. Brain 2001; 124: 1362–72.

Elenes S, Auerbach A. Desensitization of diliganded mouse muscle nicotinic acetylcholine receptor channels. J Physiol (Lond) 2002; 541: 367–83.

Engel AG. Quantitative morphological studies of muscle. In: Engel AG, Franzini-Armstrong C, editors. Myology. New York: McGraw-Hill; 1994a. p. 1018–45.

Engel AG. The muscle biopsy. In: Engel AG, Franzini-Armstrong C, editors. Myology. New York: McGraw-Hill; 1994b. p. 822–31.

Engel AG, Nagel A, Walls TJ, Harper CM, Waisburg HA. Congenital myasthenic syndromes. I. Deficiency and short open-time of the acetylcholine receptor. Muscle Nerve 1993; 16: 1284–92.

Engel AG, Lindstrom JM, Lambert EH, Lennon VA. Ultrastructural localization of the acetylcholine receptor in myasthenia gravis and in its experimental autoimmune model. Neurology 1977; 27: 307–15.

Engel AG, Ohno K, Sine SM. Sleuthing molecular targets for neurological diseases at the neuromuscular junction. Nat Rev Neurosci 2003; 4: 339–52.

Gensler S, Sander A, Korngreen A, Traina G, Giese G, Witzemann V. Assembly and clustering of acetylcholine receptors containing GFP-tagged ε or γ subunits. Selective targeting to the neuromuscular junction *in vivo*. Eur J Biochem 2001; 268: 2209–17.

Hatton CJ, Shelley C, Brydson M, Beeson D, Colquhoun D. Properties of the human muscle nicotinic receptor, and of the slow-channel myasthenic syndrome mutant εL221F, inferred from maximum likelihood fits. J Physiol (Lond) 2003; 547: 729–60.

Huebsch KA, Maimone MM. Rapsyn-mediated clustering of acetylcholine receptor subunits requires the major cytoplasmic loop of the receptor subunits. J Neurobiol 2003; 54: 486–501.

Hutchinson DO, Walls TJ, Nakano S, Camp S, Taylor P, Harper CM, et al. Congenital endplate acetylcholinesterase deficiency. Brain 1993; 116: 633–53.

Le Novère N, Corringer PJ, Changeux J-P. Improved secondary structure predictions for a nicotinic receptor subunit: incorporation of solvent accessibility and experimental data into a two-dimensional representation. Biophys J 1999; 76: 2329–45.

Luther MA, Schoepfer R, Whiting P, Casey B, Blatt Y, Montal MS, et al. A muscle acetylcholine receptor is expressed in the human cerebellar medulloblastoma cell line TE671. J Neurosci 1989; 9: 1082–96.

Maimone MM, Merlie JP. Interaction of the 43 kd postsynaptic protein with all subunits of the muscle nicotinic acetylcholine receptor. Neuron 1993; 11: 53–66.

Milone M, Hutchinson DO, Engel AG. Patch-clamp analysis of the properties of acetylcholine receptor channels at the normal human endplate. Muscle Nerve 1994; 17: 1364–9.

Milone M, Wang H-L, Ohno K, Prince RJ, Shen X-M, Brengman JM, et al. Mode switching kinetics produced by a naturally occurring mutation in the cytoplasmic loop of the human acetylcholine receptor ε subunit. Neuron 1998; 20: 575–88.

Milone M, Shen X-M, Ohno K, Harper CM, Fukudome T, Stilling G, et al. Unusual congenital myasthenic syndrome with endplate AChR deficiency caused by alpha subunit mutations and a remitting-relapsing course. Neurology 1999; 52 Suppl. 2: 185–6.

Miyazawa A, Fujiyoshi Y, Unwin N. Nicotinic acetylcholine receptor at 4.6 Å resolution: transverse tunnels in the channel wall. J Mol Biol 1999; 288: 765–86.

Miyazawa A, Fujiyoshi Y, Unwin N. Structure and gating mechanism of the acetylcholine receptor pore. Nature 2003; 423: 949–55.

Ohno K, Wang H-L, Milone M, Bren N, Brengman JM, Nakano S, et al. Congenital myasthenic syndrome caused by decreased agonist binding affinity due to a mutation in the acetylcholine receptor ε subunit. Neuron 1996; 17: 157–70.

Ohno K, Quiram P, Milone M, Wang H-L, Harper CM, Pruitt JN, et al. Congenital myasthenic syndromes due to heteroallelic nonsense/missense mutations in the acetylcholine receptor ε subunit gene: identification and functional characterization of six new mutations. Hum Mol Genet 1997; 6: 753–66.

Ohno K, Milone M, Shen X-M, Engel AG. A frameshifting mutation in CHRNE unmasks skipping of the preceding exon. Hum Mol Genet 2003; 12: 3055–66.

Plomp JJ, van Kempen GTH, Molenaar PC. Adaptation of quantal content to decreased postsynaptic sensitivity at single endplates in α-bungarotoxin treated rats. J Physiol (Lond) 1992; 458: 487–99.

Plomp JJ, van Kempen GTH, De Baets MB, Graus YMF, Kuks JBM, Molenaar PC. Acetylcholine release in myasthenia gravis: regulation at single end-plate level. Ann Neurol 1995; 37: 627–36.

Popot JL, Changeux J-P. Nicotinic receptor of acetylcholine: structure of an oligomeric integral membrane protein. Physiol Rev 1984; 64: 1162–239.

Qin F, Auerbach A, Sachs F. Estimating single-channel kinetic parameters from idealized patch-clamp data containing missed events. Biophys J 1996; 70: 264–80.

Quiram P, Ohno K, Milone M, Patterson MC, Pruitt NJ, Brengman JM, et al. Mutation causing congenital myasthenia reveals acetylcholine receptor β/δ subunit interaction essential for assembly. J Clin Invest 1999; 104: 1403–10.

Salamone FN, Zhou M, Auerbach A. A re-examination of adult mouse nicotinic acetylcholine receptor channel activation kinetics. J Physiol (Lond) 1999; 516: 315–30.

Schoepfer R, Luther MA, Lindstrom J. The human medulloblastoma cell line TE671 expresses a muscle-like acetylcholine receptor. Cloning of the alpha-subunit cDNA. FEBS Lett 1988; 226: 235–40.

Shen X-M, Ohno K, Fukudome T, Tsujino A, Brengman JM, De Vivo DC, et al. Congenital myasthenic syndrome caused by low-expressor fast-channel AChR δ subunit mutation. Neurology 2002; 59: 1881–8.

Shen X-M, Ohno K, Tsujino A, Brengman JM, Gingold M, Sine SM, et al. Mutation causing severe myasthenia reveals functional asymmetry of AChR signature Cys-loops in agonist binding and gating. J Clin Invest 2003; 111: 497–505.

Sieb JP, Kraner S, Rauch M, Steinlein OK. Immature end-plates and utrophin deficiency in congenital myasthenic syndrome caused by epsilon-AChR subunit truncating mutations. Hum Genet 2000; 107: 160–4.

Sigworth FJ, Sine SM. Data transformation for improved display and fitting of single-channel dwell time histograms. Biophys J 1987; 52: 1047–54.

Sine SM. Molecular dissection of subunit interfaces in the acetylcholine receptor: identification of residues that determine curare selectivity. Proc Natl Acad Sci USA 1993; 90: 9436–40.

Sine SM, Taylor P. Functional consequences of agonist mediated state transitions in the cholinergic receptor. Studies in cultured muscle cells. J Biol Chem 1979; 254: 3315–25.

Uchitel O, Engel AG, Walls TJ, Nagel A, Atassi ZM, Bril V. Congenital myasthenic syndromes. II. A syndrome attributed to abnormal interaction of acetylcholine with its receptor. Muscle Nerve 1993; 16: 1293–301.

Wang H-L, Milone M, Ohno K, Shen X-M, Tsujino A, Batocchi AP, et al. Acetylcholine receptor M3 domain: stereochemical and volume contributions to channel gating. Nat Neurosci 1999; 2: 226–33.

Wang H-L, Ohno K, Milone M, Brengman JM, Evoli A, Batocchi AP, et al. Fundamental gating mechanism of nicotinic receptor channel revealed by mutation causing a congenital myasthenic syndrome. J Gen Physiol 2000; 116: 449–60.

Yu X-M, Hall ZW. The role of the cytoplasmic domains of individual subunits of the acetylcholine receptor in 43 kDa protein-induced clustering in COS cells. J Neurosci 1994; 14: 785–95.

Viral vector-medicated expression of human collage Q in cultured cells

Mikako Ito[a], Akio Masuda[a], Shinsuke Jinno[a], Takeshi Katagiri[a], Eric Krejci[b], Kinji Ohno[a]*

[a]Division of Neurogenetics, Center for Neurological Diseases and Cancer, Graduate School of Medicine, Nagoya University, 65 Tsurumai, Showa-Ku, Nagoya, 466-8550, Japan

[b] INSERM U686, Biologie des Jonctions Neuromusculaires Normales et Pathologiques, Université René Descartes, 45 rue des Saints-Pères, Paris, F-75006, France

*Corresponding author. Tel.: +81 52 744 2447; fax: +81 52 744 2449.

E-mail address: ohnok@med.nagoya-u.ac.jp (K. Ohno).

Abstract

Congenital myasthenic syndromes are caused by mutations in molecules expressed at the neuromuscular junction. Collagen Q (ColQ) makes a triple helical structure and anchors the catalytic subunit of acetylcholinesterase (AChE) to the synaptic basal lamina in the form of asymmetric AChE. Mutations in the collagen Q gene (*COLQ*) cause endplate AChE deficiency. As an initial step to develop a novel therapeutic strategy for endplate acetylcholinesterase deficiency, we expressed AChE species in cultured cells delivered by retrovirus and adeno-associated virus (AAV).

The retroviral vectors carried human *ACHE* and *COLQ* either in a single construct (EF1α-*ACHE*-IRES-*COLQ*) or in two separate constructs (EF1α-*ACHE* and EF1α-*COLQ*). We produced high-titer retroviruses using the PLAT-E retrovirus packaging cells. We also confirmed expression of asymmetric AChE in the PLAT-E cells. We infected NIH3T3 and confirmed expression of the transgenes by RT-PCR. The AAV vector carried human *COLQ*-IRES-*EGFP* downstream of the CMV promoter (pAAV-CMV-*COLQ*-IRES-*EGFP*). We produced recombinant AAV using HEK293 cells carrying pDF6 encoding the AAV6 capsid gene. We infected AAVHT1080 cells and confirmed expression of *COLQ* by RT-PCR and EGFP by flow cytometry. We are currently working on achieving further higher expression levels of transgenes in cultured cells to make the current strategy applicable to an animal model.

Keywords: collagen Q; acetylcholinesterase; retrovirus; adeno-associated virus

Introduction

There has been no rational therapy for endplate acetylcholinesterase deficiency caused by a congenital defect of collagen Q (ColQ). Unlike other molecules defective in congenital myasthenic syndromes, ColQ is an extracellular matrix protein [1]. Asymmetric acetylcholinesterase (AChE) harboring the ColQ is excreted from muscle cells and is precisely anchored to the synaptic basal lamina [2].

We tried to exploit these features of the asymmetric acetylcholinesterase to develop a novel therapeutic strategy for endplate acetylcholinesterase deficiency. As an initial step of this strategy, we here report retrovirus vector-mediated expression of collagen-tailed AChE, as well as adeno-associated virus (AAV)-mediated expression of ColQ.

Materials and methods

Retrovirus vectors

We inserted an EF1α promoter into the pSIREN-RetroQ retroviral vector (Clonetech). We then inserted either human *ACHE* to make pSIREN-EF1α-*ACHE*, human *COLQ* to make pSIREN-EF1α-*COLQ*, or human *ACHE*, IRES, and human *COLQ* to make pSIREN-EF1α-*ACHE*-IRES-*COLQ*. We employed PLAT-E packaging cells (a kind gift of Dr. Toshio Kitamura, Univ. of Tokyo) to produce recombinant retrovirus particles. PLAT-E cells were transfected with retroviral vectors using FuGENE6 (Roche). Sedimentation analysis was performed in a 5-20% sucrose density gradient to separate AChE

species from mouse muscle and PLAT-E cells as described previously [3]. The virus titers for NIH3T3 cells were ~1.6 x 10^7 PFU/ml. In NIH3T3 cells infected with retrovirus particles, we confirmed expression of the transgenes by RT-PCR and by Western blot analysis using anti-human ColQ polyclonal antibody (Gene way).

AAV vectors

We inserted either human *COLQ* or human *COLQ*-IRES-*EGFP* downstream of a CMV promoter in the pAAV-MCS vector (Stratagene). Adenovirus-independent helper plasmid pDF6 carrying a serotype 6 capsid was a kind gift of Dr. Mark A. Kay, Stanford University.

We cotransfected HEKT293T cells with pAAV-*COLQ* and pDF6 by the calcium phosphate precipitation method [4] to generate rAAV6-*COLQ*. We infected AAV-HT1080 cells (Stratagene) with rAAV6-*COLQ*, and confirmed expression of *COLQ* by RT-PCR.

Results and discussion

3.1 *Retrovirus-mediated expression of asymmetric AChE in cultured cells*

PLAT-E cells were transfected with pSIREN-*ACHE*-IRES-*COLQ* to yield virus particles. In these cells, we observed production of both globular and asymmetric forms of AChE, as we can see in wild-type mouse skeletal muscles by sedimentation analysis in sucrose gradients (Fig.1).

We next infected NIH3T3 cells with the *ACHE*-IRES-*COLQ* retrovirus, or with both the *ACHE* and *COLQ* retroviruses. In both cells, we confirmed expression

of the transgene mRNAs and proteins. We also observed secretion of ColQ in culture medium by Western blotting (data not shown).

3.2 *AAV-mediated expression of ColQ in cultured cells*

rAAV6-*COLQ* harbors serotype 6, and should have tropism for skeletal muscles. In AAV-HT1080 cells infected with rAAV6-*COLQ*-IRES-*EGFP*, we observed expressions of *COLQ* mRNA by RT-PCR, and of EGFP by flow cytometry (data not shown). We administered ~1 x 10^8 vector genomes in the tail vein of a *ColQ*-knockout mouse. We are currently observing if the AAV vector shows any beneficial effects on the treated mouse.

3.3 *Future perspectives*

In this study, we demonstrate that the recombinant retrovirus and AAV efficiently express transgenes in cultured cells. We are currently working on achieving further higher expression levels of transgenes in cultured cells, as well as in culture medium. Through the current strategy, we hope to ameliorate motor symptoms of the knockout mice [5] and of the patients.

Acknowledgments

The research was supported by Grants-in-Aid for Scientific Research from the Japan Foundation for Neuroscience and Mental Health.

References

[1] K. Ohno, A.G. Engel, J.M. Brengman, X.M. Shen, F. Heidenreich, A. Vincent,

M. Milone, E. Tan, M. Demirci, P. Walsh, S. Nakano, I. Akiguchi, The spectrum of mutations causing end-plate acetylcholinesterase deficiency, Ann. Neurol. 47 (2000) 162-170

[2] L.M. Kimbell, K. Ohno, A.G. Engel, R.L. Rotundo, C-terminal and heparin-binding domains of collagenic tail subunit are both essential for anchoring acetylcholinesterase at the synapse, J. Biol. Chem. 279 (2004) 10997-11005

[3] K. Ohno, J. Brendman, A. Tsujino, A.G. Engel, Human endplate acetylcholinesterase deficiency caused by mutations in the collagen-like tail subunit (ColQ) of the asymmetric enzyme, Proc. Natl. Acad. Sci. USA 95 (1998) 9654-9659

[4] T. Okada, T. Nomoto, K. Shimazaki, W. Lijun, Y. Lu, T. Maatsushita, H. Mizukami, M. Urabe, Y. Hanazono, A. Kume, S. Muramatsu, I. Nakano, K. Ozawa, Adeno-associated virus vectors for gene transfer to the brain, Methods 28(2) (2002) 237-247

[5] G. Feng, E. Krejci, J. Molgo, J.M. Cunningham, J. Massoulie, J.R. Sanes, Genetic analysis of collagen Q: Roles in acetylcholinesterase and butyrylcholinesterase assembly and in synaptic structure and function, J. Biol. Chem. 144 (1999) 1349-1360

Figure Legend

Fig. 1. Sedimentation profiles of AChE species. (A) In wild-type mouse, we observe both asymmetric and globular forms of AChE. (B) In ColQ-deficient mice [4], no asymmetric AChE species are formed. (C) In PLAT-E cells transfected with pSIREN-*ACHE* alone, only globular forms are generated. (D) In PLAT-E cells transfected with pSIREN-*ACHE*-IRES-*COLQ*, both asymmetric and globular forms are generated.

Fig. 1.

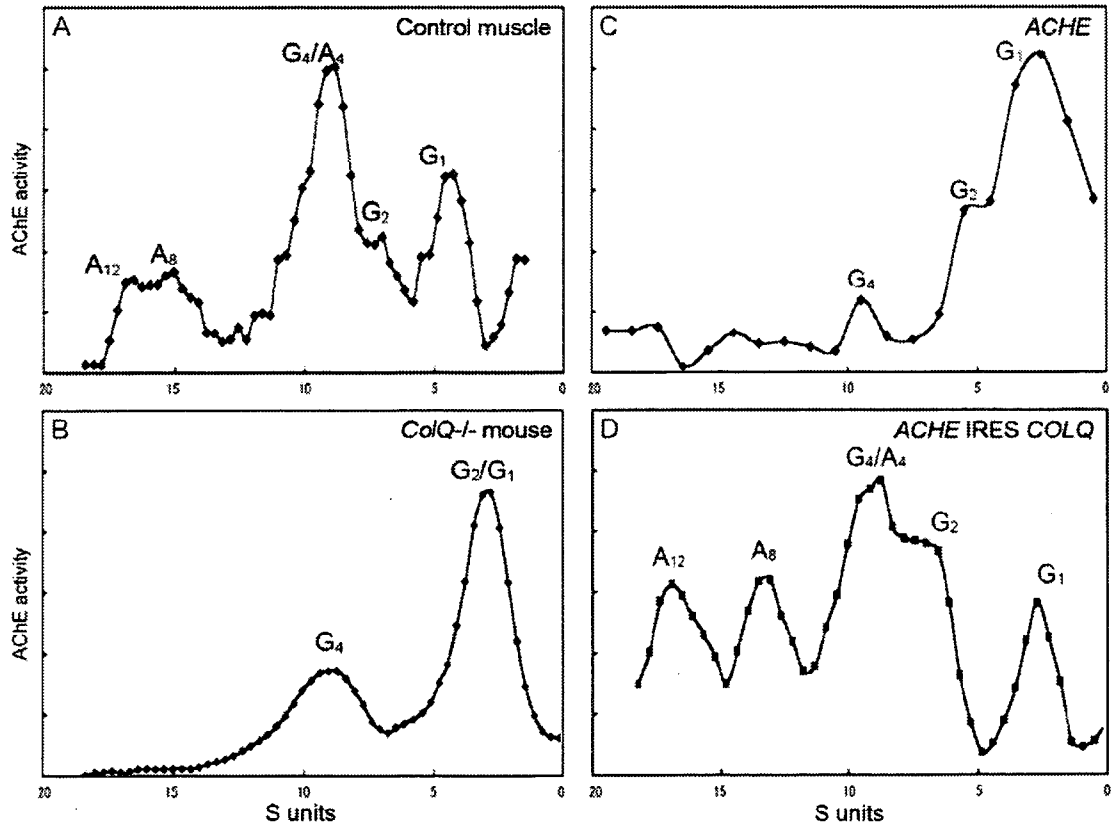

Novel AChR δ subunit mutation causing myasthenia hinders intersubunit link essential for channel gating

Xin-Ming Shen,[1] Taku Fukuda,[1] Kinji Ohno,[1] Steven M. Sine,[2] and Andrew G. Engel[1]

[1]Muscle Research Laboratory, Department of Neurology; and [2]Receptor Biology Laboratory, Department of Physiology and Biophysics, Mayo Clinic, Rochester, MN 55905

Dr. Fukuda's current address is First Department of Internal Medicine, Nagasaki University Hospital, Nagasaki, Japan; Dr. Ohno's current address is Department of Neurogenetics and Bioinformatics, Nagoya University Graduate School of Medicine, Nagoya, Japan.

Address correspondence to Andrew G. Engel, Department of Neurology, Mayo Clinic, Rochester MN 55905. Phone: 507-284-5102; Fax: 507-284-5831; E-mail: age@mayo.edu.

Nonstandard abbreviations used in text: CMS, congenital myasthenic syndrome, EP, endplate; EPP, endplate potential; HEK, human embryonic kidney; MEPC, miniature EP current; MEPP miniature EP potential.

Abstract

We trace the cause of a congenital myasthenic syndrome associated with endplate AChR deficiency and low amplitude synaptic potentials to the hetero-allelic mutations δL42P and δI58K. We find that δI58K abolishes AChR expression by impairing association of α- and δ-subunits, whereas δL42P enables low expression but severely attenuates channel gating, thus determining the phenotype. AChRs containing δL42P exhibit shortened bursts of channel openings elicited by a low ACh concentration, predicting accelerated decay of the synaptic response, and a reduced probability the di-liganded AChR channel will open, accounting for reduced response amplitude. Substitutions of Gly, Lys, and Asp for δL42, or of Pro for δN41, δI43, and δS44 similarly attenuate channel gating. Mutation of residues equivalent to δL42 in the ε, α, and β subunits impede, do not significantly affect, and enhance the response to ACh, indicating the mutated region contributes to channel gating in a subunit specific manner. Thermodynamic mutant cycle analyses reveal strong energetic coupling between δL42 and Y127 from the opposing α-subunit, which forms an inter-subunit linkage with δN41 known to be crucial for channel gating. Our overall findings indicate δL42P perturbs its constituent β-strand of the δ-subunit, disrupting the inter-subunit linkage between δN41 and αY127 required for rapid and efficient channel gating.

Introduction

Congenital myasthenic syndromes (CMSs) are heterogeneous disorders caused by defects in presynaptic, synaptic, or postsynaptic proteins (1). Targets for CMS mutations include choline acetyltransferase (2), the collagenic tail subunit of the end-plate species of acetylcholinesterase (3, 4), rapsyn (5), the $Na_v1.4$ sodium channel (6), the muscle-specific receptor tyrosine kinase (MuSK) (7), Dok-7, the muscle-intrinsic activator of MuSK (8), and the nicotinic acetylcholine receptor (AChR) (9). Most postsynaptic CMS are caused by mutations in different subunits of AChR that alter its kinetics of activation by ACh, reduce its expression, or both.

AChR is a ligand-gated ion channel with a pentameric structure consisting of four homologous subunits with a stoichiometry $\alpha_2\beta\delta\gamma$ in the fetus or $\alpha_2\beta\delta\varepsilon$ in the adult. Each AChR subunit has a large N-terminal extracellular domain, four transmembrane domains, an extracellular linker and two intracellular domains (10). The extracellular domain of each subunit consists largely of β-strands that twist to form a β-sandwich, creating a conserved hydrophobic core within each subunit and highly complementary subunit interfaces, two of which form the ligand binding sites (11). The β_1 through β_6 strands compose the inner sheets of the β-sandwich, with the β_7 through β_{10} strands forming the outer sheets. A disulfide bond of the signature cys-loop links the two sheets together (11, 12). At interfaces that form the agonist binding sites, the β_1 strand from the inner sheets of the δ- and ε-subunits approaches the junction of the inner and outer sheets of the neighboring α-subunit. At this inter-subunit interface, Asn 41 in the δ subunit and the equivalent Asn 39 in the ε subunit couple energetically with Tyr 127 in the α-subunit to form an inter-subunit link essential for channel gating (13). However, whether other residues in β_1 strands of the δ and ε subunits contribute to the inter-subunit link is not known, and to date no naturally occurring mutations have been detected in any AChR β_1 strand.

We here trace the cause of a CMS to two pathogenic mutations in the AChR δ subunit: δL42P in the β_1 strand which causes abnormally brief channel openings, and δI58K in the β_2 strand which hinders AChR assembly. The principle effect of δL42P is to attenuate channel gating by reducing both its speed and efficiency. Thermodynamic mutant cycle analysis reveals that the functional consequences of δL42P result from structural perturbation of an inter-subunit link between α- and δ-subunits essential for channel gating.

Results

Characteristics of CMS patient. A 20-year-old woman had moderately severe to severe myasthenic symptoms since birth, no anti-AChR antibodies, and a 34-71% decremental response of the compound muscle action potential on repetitive stimulation of motor nerves at 2 Hz. She responded poorly to pyridostigmine alone but improved markedly after the addition of 3,4-diaminopyridine. A similarly affected sibling died at age 11 months.

Endplate studies. The configuration of the endplates (EPs), evaluated from the cytochemical reaction for acetylcholinesterase on longitudinally oriented teased single muscle fibers, was abnormal, with numerous small EP regions distributed over a 2- to 4-fold increased span of the muscle fiber surface. The reaction for AChR, detected in cryostat sections with rhodamine-labeled α-bungarotoxin (α-bgt) was greatly attenuated.

On EM, the structural integrity of the junctional folds was preserved. Morphometric analysis of individual EP regions revealed that nerve terminal size was normal but the postsynaptic area of junctional folds and cleft was reduced to 58% of normal. Some postsynaptic regions were simplified and the postsynaptic membrane length per unit postsynaptic area was 70% of normal. The reaction for AChR, detected with peroxidase-labeled α-bgt, was patchy as well as attenuated (Figure 1) and the AChR-reactive postsynaptic membrane length was 33% of normal (Table 1). The number of ^{125}I α-bgt sites per EP was decreased to 16% of normal (Table 2).

In vitro microelectrode studies of intercostal muscle EPs showed that quantal release by nerve impulse was normal. The miniature EP potential (MEPP) and current (MEPC) amplitudes were reduced to 6% and 10% of normal, respectively (Table 2).

Mutation analysis. Direct sequencing of each AChR subunit gene revealed three heterozygous mutations in CHRND: 125T>C, predicting Leu>Pro at codon 42 (δL42P) in the β_1 strand; 173T>A, predicting an Ile>Lys at codon 58 (δI58K) in the β_2 strand, and 277G>C predicting Val>Leu at codon 93 (δV93L) in the β_4 strand (Figure 2A). δL42 and δV93L are conserved across AChR δ subunits of different species; I58K is conserved in δ subunits of mammals, and in human ε and γ subunits (Fig 2A). None of the mutations is present in 200 normal alleles of 100 unrelated subjects. Family analysis indicates that each mutation is recessive with δI58K and δV93L in the paternal and δL42P in the maternal allele (Figure 2B).

Expression studies of mutant AChRs expressed in HEK cells. To determine whether the mutations hinder the surface expression of AChR, we engineered the observed mutations into the human δ subunit and coexpressed them with complimentary wild-type α, β, and ε subunits in HEK cells. As controls, we coexpressed wild-type α, β, δ, and ε subunits, and also wild-type α, β, and ε subunits without the δ subunit. Compared to wild-type, surface [^{125}I]α-bgt binding was enhanced by δV93L, reduced to 37% by δL42P, and decreased to 5% by δI58K and by the δ-omitted $\alpha_2\beta\varepsilon_2$ construct (Figure 3A). Surface expression of the double mutant δI58K+V93L-AChR was similar to that of δI58K-AChR, indicating that δV93L did not mitigate the effects of δI58K (Figure 3A). We also compared expression of the wild α/δ dimer with that harboring δI58K, and with expression of only the α subunit. Toxin binding by HEK cells expressing the mutant dimer was only 15% of that of the wild-type dimer and not different from toxin binding by HEK cells expressing only the α subunit (Figure 3B), indicating that δI58K hinders δ/α subunit association, an early step in AChR assembly (14). We also compared the apparent affinity for ACh of the δL42P receptor relative to wild-type by measuring ACh binding at steady state by competition against the initial rate of [^{125}I]α-bgt binding to intact cells (15). The apparent dissociation constant of δL42P-AChR was reduced 5-